

Superconducting heterostructures: from antipinning to pinning potentials

S J Carreira^{1,3}, C Chilotte¹, V Bekeris¹, Y J Rosen^{2,4}, C Monton² and Ivan K Schuller²

¹Departamento de Física, FCEyN, Universidad de Buenos Aires and IFIBA, CONICET, Pabellón 1, Ciudad Universitaria, 1428 Buenos Aires, Argentina

²Physics Department, University of California-San Diego, La Jolla, CA 92093-0319, USA

E-mail: vbekeris@df.uba.ar

Received 28 March 2014, revised 30 April 2014

Accepted for publication 28 May 2014

Published 2 July 2014

Abstract

We study vortex lattice dynamics in a heterostructure that combines two type-II superconductors: a niobium film and a dense triangular array of submicrometric vanadium (*V*) pillars. Magnetic ac susceptibility measurements reveal a sudden increase in ac penetration, related to an increase in vortex mobility above a magnetic field, $H^*(T)$, that decreases linearly with temperature. Additionally, temperature independent matching effects that occur when the number of vortices in the sample is an integer of the number of *V* pillars, strongly reduce vortex mobility, and were observed for the first and second matching fields, H_1 and H_2 . The angular dependence of H_1 , H_2 and $H^*(T)$ shows that matching is determined by the normal applied field component, while $H^*(T)$ is independent of the applied field orientation. This important result identifies $H^*(T)$ with the critical field boundary for the normal to superconducting transition of *V* pillars. Below $H^*(T)$, superconducting *V* pillars repel vortices, and the array becomes an ‘antipinning’ landscape that is more effective in reducing vortex mobility than the ‘pinning’ landscape of the normal *V* sites above $H^*(T)$. Matching effects are observed both below and above $H^*(T)$, implying the presence of ordered vortex configurations for ‘antipinning’ or ‘pinning’ arrays.

Keywords: superconductor, type II, heterostructure

(Some figures may appear in colour only in the online journal)

1. Introduction

The effect of artificial pinning centers on the behavior of the vortex lattice (VL) in superconducting systems has been an issue of intense research over the past decades. Engineering samples with controlled pinning arrays in the nm length scale have assisted an active feedback between detailed calculations and experiments to examine the response of the VL moving in specific pinning landscapes. For applications, the strong attention in these systems is mainly to control crucial

parameters such as critical current, creep or magnetization, all strongly influenced by pinning forces.

In the presence of periodic arrays of pinning centers, vortex dynamics show interesting commensurate or matching effects when the number of vortices is an integer or a fraction of the number of pinning sites, leading to a strong enhancement of the critical current and a strong decrease in vortex mobility and ac penetration. Attention has been mainly focused on regular arrays of holes (antidots) [1], blind holes [2] and magnetic [3] or non-magnetic normal dots [4].

Recently, however, the stable vortex structures in thin superconducting films containing superconducting pillars have been studied [5] and the transport in superconducting films with modulated thickness [6] examined. It has been shown that superconducting pillars repel vortices [7], making the array an ‘antipinning’ periodic landscape that may be

³ Current address: Depto. de Materia Condensada, Centro Atómico Constituyentes, CNEA, Av. Gral Paz 1499 (1650), Partido de San Martín, Prov. de Buenos Aires, Argentina

⁴ Current address: Laboratory for Physical Sciences, College Park, MD 20740, USA

viewed as the inverse type of defects to a lattice of antidots or of normal pinning dots.

In this paper we examine the VL dynamics in a niobium (Nb) film containing a dense submicrometric triangular array of vanadium (V) pillars, with a bulk superconducting critical temperature, T_{C0}^V , and upper critical field, $H_{C2}^V(0)$, respectively lower than the bulk T_{C0}^{Nb} and H_{C2}^{Nb} of Nb. The VL behavior was studied using ac susceptibility measurements, $\chi_{ac} = \chi' + j\chi''$, as a function of temperature and magnetic field.

In addition to temperature independent matching effects, we find that at a temperature dependent magnetic field, $H^*(T)$, an abrupt change in the dynamics of the VL occurs and mobility suddenly increases with field. Through angular dependent measurements we identify $H^*(T)$ with the critical field or $H-T$ phase boundary for the normal to superconducting transition of V pillars. In this scenario, superconducting V pillars, known to repel vortices [7], form an antipinning landscape [5] below $H^*(T)$, and above this field become normal attractive pinning centers, inducing a local depression of the superconducting parameter in the Nb film by proximity effects. We find that for the geometry of our samples, antipinning is more efficient than pinning in reducing VL mobility and matching effects occur in both cases. The paper is organized as follows. In section 2 we describe the experimental details, and results and discussions are presented in section 3. Conclusions are drawn in section 4.

2. Experimental

A dense submicrometric triangular array of V pillars, diameter $d = (70 \pm 5)$ nm and thickness $h = (40 \pm 2)$ nm with lattice parameter $D = (100 \pm 10)$ nm, was deposited on a Si substrate as described elsewhere [8]. On top of the V dots, a Nb film of thickness $t = (100 \pm 5)$ nm was sputtered. The bulk critical temperature of V, $T_{C0}^V = 5.4$ K [9], is lower than the bulk critical temperature of Nb, $T_{C0}^{Nb} = 9$ K [10], although it is well known that critical temperature may be strongly modified for films or heterostructures [11], particularly in this case where the absence of an insulating layer between the Nb film and the V pillars gives rise to strong proximity effects.

The sample is (2×3.5) mm². Figure 1 shows two scanning electron microscopy images of the sample, magnified 50 000 in panel (a) and 400 000 times in panel (b), where the triangular array of V pillars is observed. The images were taken rotating the sample 30° from the beam direction to observe the pillars more clearly.

It is well known that for a triangular array of strong pinning potentials with lattice parameter D , the calculated first and second matching fields are $H_1^C = 2\phi_0/\sqrt{3}D^2 = (2390 \pm 480)$ Oe, and $H_2^C = 4\phi_0/\sqrt{3}D^2 = (4780 \pm 960)$ Oe, with the flux quantum $\phi_0 = 2.07 \cdot 10^{-7}$ Gcm².

Ac susceptibility, $\chi_{ac}(H, T) = \chi'(H, T) + j\chi''(H, T)$, is a complex magnitude and is a property of the sample, not

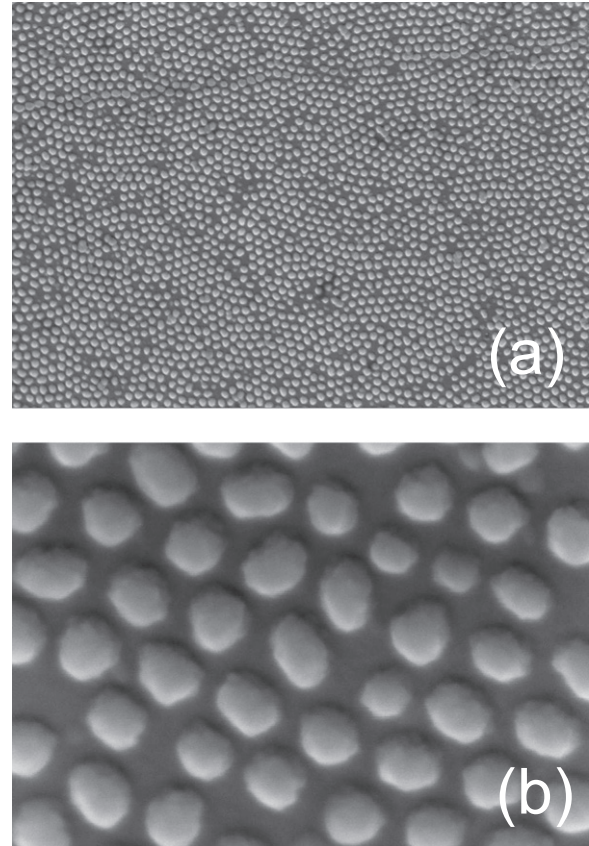


Figure 1. SEM image of the sample showing the Nb film containing the triangular array of V pillars. (a) $\times 50\,000$ and (b) $\times 400\,000$. The sample was rotated 30° from the beam direction to observe the V pillars.

only of the material, because it is related to the induced currents, $j(t)$, that define the time dependent magnetization $M(t) = \frac{1}{2cv} \int_V r \times j(t) dv$, where v is the sample volume and boundary conditions intervene. If a dc magnetic field, superposed to an ac magnetic field, $H_T = H + h_{ac} \cos(\omega t)$, is applied to a superconductor, due to the induced shielding currents, $M(t)$ is periodic in $2\pi/\omega$. The first Fourier components of $M(t)$ are χ' and χ'' . The ac susceptibility real component χ' is in phase with magnetization and therefore it is in direct relation to the penetration of ac field in the sample. The out of phase component χ'' is related to the dissipation due to the electric field induced by changes in the magnetic flux in the sample. Measurements were performed in a commercial QD MPMS XL 7 T magnetometer. An applied ac magnetic field, h_{ac} , modulates the dc field, H , that creates vortices inside the sample and $\chi_{ac}(H, T)$ is measured using an array of secondary coils. In the non-linear regime, vortices perform excursions outside the effective pinning wells, $\chi_{ac}(H, T)$ is h_{ac} dependent and ac losses are not negligible. A small ac penetration depth or high screening ($\chi'(H, T) \cong -1$), is related to a VL with low mobility. In contrast, a large ac penetration depth ($\chi'(H, T) \cong 0$) results for a weakly pinned, highly mobile VL. Losses on the other hand tend to zero for highly screened ac fields that produce no changes in the

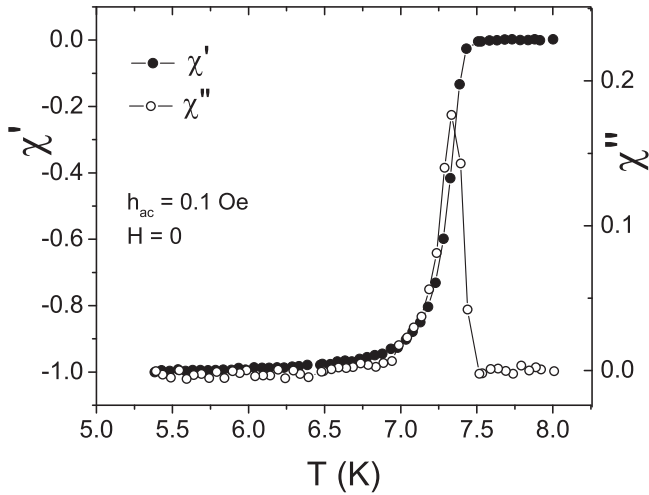


Figure 2. Screening $\chi'(T)$ (full symbols, left axis) and losses, $\chi''(T)$ (open symbols, right axis) at zero dc field for $h_{ac} = 0.1$ Oe and $f = 1$ kHz.

magnetic flux in the sample and also for high ac penetration where magnetization is zero. Therefore χ'' shows a peak as a function of dc field or temperature. For H and T below the peak, an increase in χ'' implies an increase in VL mobility or a decrease in effective pinning.

The applied ac amplitude was $h_{ac} = 1$ Oe and the frequency $f = 1$ kHz, except to determine the critical onset temperature and transition width, where the applied ac field was reduced to $h_{ac} = 0.1$ Oe. Ac and dc magnetic fields were applied perpendicular to the samples, except for the angle dependent measurements that will be described below.

3. Results and discussion

Figure 2 shows the zero field temperature dependence of ac susceptibility, $\chi'(T)$ (full symbols, left axis) and $\chi''(T)$ (open symbols, right axis), for $h_{ac} = 0.1$ Oe. The sample critical temperature determined with this technique is $T_{C0} = (7.49 \pm 0.02)$ K with a 10–90% transition width $\Delta T_C = 0.2$ K.

One of the main results of our paper is shown in figure 3, where we plot in panel (a) $\chi''(H)$ for zero field cooled samples at different temperatures, 3.0, 3.9, 4.7, 5.2, 5.3, 5.5, 5.6, 5.7, 5.9 and 6.0 K. Temperature control was in the mK throughout the measurements. Vertical lines indicate the experimental first and second matching fields, $H_1 = (2020 \pm 50)$ Oe and $H_2 = (4050 \pm 50)$ Oe in good agreement with calculated values, for one and two flux quanta per array cell respectively. Calculated vortex ground states obtained from simulated annealing for a triangular pinning array for the first matching fields are shown for example in figure 2 of [12]. Matching effects, where pinning becomes more effective, are clearly observed at the higher temperatures ($T \geq 5.6$ K). For intermediate temperatures, $5.2 \text{ K} \leq T \leq 5.6$ K, the first matching is blurred, but the

second matching field is clearly observed. At low temperature, for 3.9 K and 4.7 K, weak commensurate effects for H_1 and H_2 , respectively are observed (see figures 3(c) and 4(a)). The periodicity in the pinning landscape is known to be smeared at low temperatures because intrinsic random pinning increases as the temperature is reduced. The response is reversible in field at constant temperature, an indication that intrinsic pinning is not strongly competing with artificial pinning in our temperature window, and is not generating different metastable vortex configurations [13].

A salient feature is observed in figure 3: $\chi''(H)$ increases with magnetic field at a temperature dependent rate, but above a cross over field, $H^*(T)$, that depends on temperature and is indicated by short vertical arrows in the three panels, the rate is suddenly modified and the ac penetration depth grows faster with magnetic field, i.e. the rate increases. This is an indication of an abrupt variation in the pinning mechanism that is more effective below $H^*(T)$ than above it. For clarity, in panel (b) we plotted the data after subtracting a linear fit to the first five data points, $\Delta\chi''$ versus magnetic field, for $T = 5.3, 5.5, 5.6, 5.7$ and 5.9 K. For these temperatures the cross over field, $H^*(T)$, lies below the first matching field, H_1 . In panel (c) we plot $\chi''(H)$ for $T = 3.0, 3.9, 4.7$ and 5.2 K. At the lowest temperatures, matching effects are strongly blurred due to the increase in intrinsic random pinning. However a clear change in the behavior of the VL regime occurs above H_1 , and the vertical arrow indicates the cross over field, $H^*(T)$ for $T = 4.7$ K. For $T = 5.2$ K, $H^*(T)$ is probably close to H_1 , as we will see below when plotting $H^*(T)$ as a function of temperature. For $T = 3.9$ K we observe a change in VL mobility for H_2 and we believe that $H^*(T)$ is well above the second matching field (see figure 5).

In contrast to H^* matching fields H_1 and H_2 are temperature independent. Temperature dependent matching in a flux-line lattice interacting with a triangular array of pinning centers without long-range order has been addressed [14, 15]. The authors find that, for disordered arrays, matching fields shift towards lower values for lower temperatures, and trace back this weak variation with T to a temperature dependent averaging over differently ordered domains. The strong decrease in H^* with increasing T in our samples is evidence that H^* is not related to commensurability effects.

We now discuss the origin of $H^*(T)$. The sample is a combination of two bulk type-II superconducting materials, the Nb film and the array of mesoscopic V pillars. In a simplified scenario, H^* could either be the lower critical field, H_{C1} , of Nb or of V , or the upper critical field H_{C2} of V . However, the mesoscopic character of the V dots in contact with the Nb superconducting film is not straightforward to analyze. It is well known that critical fields H_{C1} and H_{C2} for isolated mesoscopic disks strongly differ from the bulk critical fields showing pseudoperiodicity and depending on the detailed form or geometry and on the boundary conditions [16].

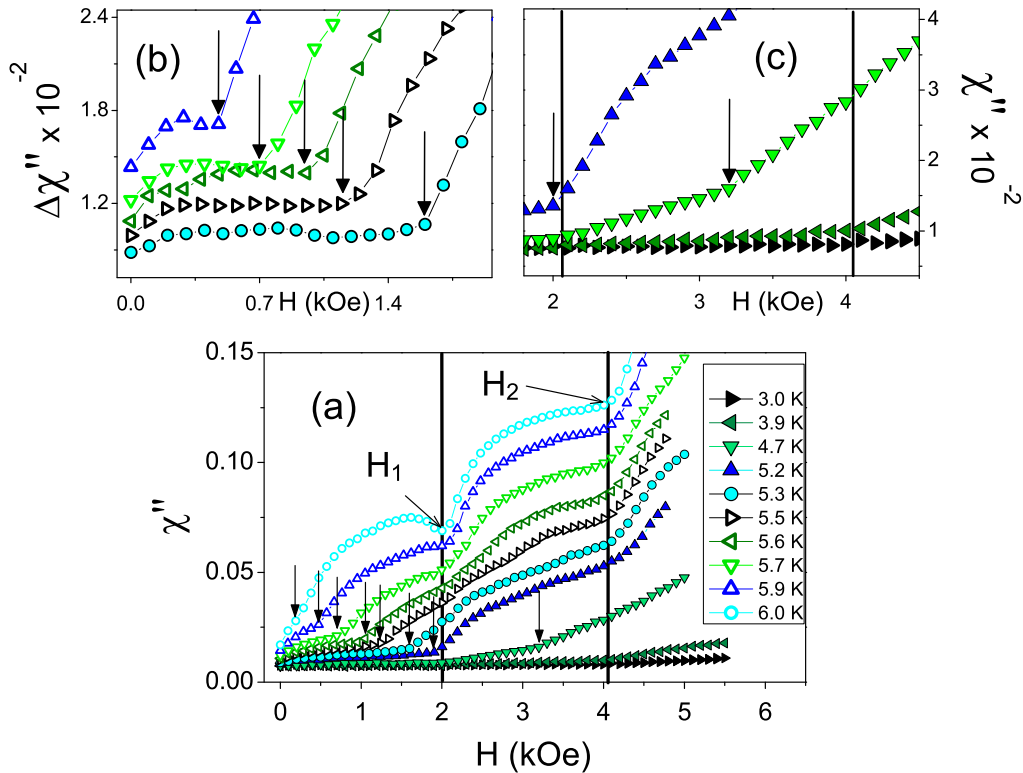


Figure 3. (a) The ac losses as a function of dc field for zero field cooled samples at different temperatures, 3.0, 3.9, 4.7, 5.2, 5.3, 5.5, 5.6, 5.7, 5.9 and 6.0 K, for $h_{ac} = 1$ Oe. Arrows indicate the field $H^*(T)$ where the behavior of the VL shows a change. Matching at $H_1 = (2020 \pm 50)$ Oe and $H_2 = (4050 \pm 50)$ Oe are shown in vertical lines. (b) $\Delta\chi''$ obtained after subtracting a linear fit to the first data points in (a) (see text). Vertical arrows indicate $H^*(T)$. (c) Details are shown for $T = 3.0, 3.9, 4.7$ and 5.2 K. The arrows indicate $H^*(T)$.

The external magnetic field H was applied perpendicular to the sample surface, therefore strong demagnetizing effects are relevant, particularly if the sample is in Meissner state. In this case, the internal field $H_{int} = H/(1 - N)$, with a demagnetizing factor for our geometry, $N \approx 1$. Therefore, we may discard the fact that $H^*(T)$ coincides with the lower critical field $H_{C1}(T)$ of the Nb film containing V dots, since in the perpendicular configuration the measured H^* would correspond to extremely high values for $H_{C1}(T)$. In addition to this argument is the fact that losses should be zero in Meissner state, while finite losses are observed below $H^*(T)$ as shown in figure 3. In the case of V pillars, we are led to discard $H_{C1}(T)$ of V pillars as the origin of $H^*(T)$, as we would expect to observe a second feature at higher field or temperature at the superconducting to normal boundary of pillars, that is absent. This leads us to propose that $H^*(T)$ is the line boundary in the $H - T$ phase diagram where V pillars become normal. An additional test is available: demagnetizing effects become negligible near the nucleation field where magnetization tends to zero, therefore no dependence of H^* with the applied field orientation should be observed.

We therefore repeated the $\chi_{ac}(H)$ measurements for magnetic fields applied at different angles θ from the normal to the sample surface, as schematically shown in the inset of figure 4. In figure 4(a) we plot $\Delta\chi''(H)$ for $T = 4.7$ K for the

field oriented normal to the sample, $\theta = 0^\circ$, (open symbols) and for $\theta = (34 \pm 5)^\circ$ (full symbols) after subtracting from $\chi''(H, \theta)$ a linear fit to the data below H^* , for clarity, as was done in figure 3(b). Data for $\theta = 0^\circ$ was displaced arbitrarily upwards and lines are plotted as a guide to the eye. In panel (b) we plot $\Delta\chi''(H)$ for $T = 5.7$ K, $\theta = 0^\circ$ and $\theta = (40 \pm 5)^\circ$, again after subtracting from $\chi''(H, \theta)$ a linear fit to the data below H^* , for clarity. Comparing at each temperature the results for the applied field normal to the sample and for the applied field oriented away from the sample normal we observe a shift in the applied matching field to higher fields with angle, $H_1^\theta = H_1^0/\cos(\theta) = 2412$ Oe and 2610 Oe for $\theta = 34^\circ$ and $\theta = 40^\circ$ respectively, and $H_2^\theta = H_2^0/\cos(\theta)$ (not shown), indicating that the perpendicular component of the magnetic field is relevant to create a number of vortices that match the number of artificial sites [17]. $H^*(T)$ does not change with the orientation of the applied field, providing evidence that it is consistent to identify H^* with the upper critical field of V pillars.

In figure 5 we plot $H^*(T)$, which shows a linear dependence with temperature; the line is a guide to the eye. However, experimental [18] and theoretical [16] results predict oscillations in the upper critical field of isolated simply connected mesoscopic superconducting disks that we do not

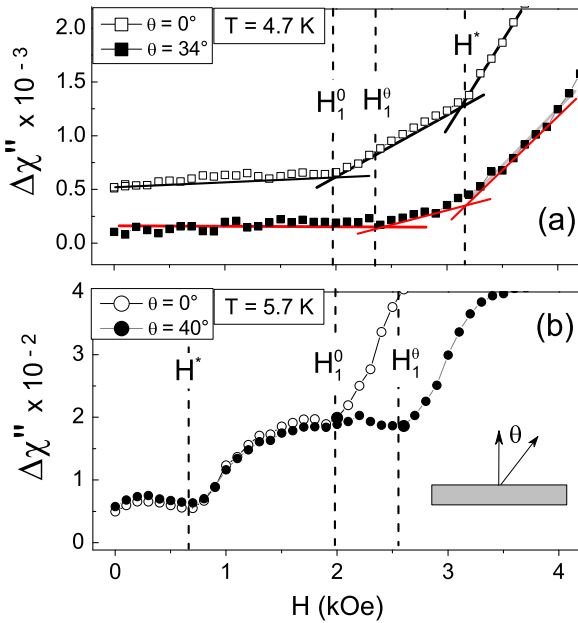


Figure 4. $\Delta\chi''(H)$ after subtracting from $\chi''(H)$ a linear fit for data below H^* for two field orientations as schematized in the inset: normal to the sample $\theta = 0^\circ$ (open symbols) and oriented from the sample normal (full symbols), for (a) $T = 4.7$ K and $\theta = (34 \pm 5)^\circ$, and (b) $T = 5.7$ K and $\theta = (40 \pm 5)^\circ$. Matching fields are shifted (see text) but H^* is angle independent. The data for $\theta = 0^\circ$ in panel (a) was shifted upwards for clarity. The lines are a guide to the eye (see text).

observe. As the sample has an array of V pillars with (narrow) distribution of sizes, this oscillatory effect may be blurred.

In our scenario, V pillars contained in the superconducting Nb film, (i.e. below the upper critical field of the film, H_{C2} , as shown the inset of figure 5) become normal for $H^*(T) < H$ and behave as an array of normal pinning centers giving rise to the commensurate effects at H_1 and H_2 clearly shown in figure 3 at high temperature. However, matching is also observed for V acting as antipinning superconducting pillars as shown in panel (c) of figure 3 and in panel (a) of figure 4, for $T = 4.7$ K where $H_1 < H^*(T)$. Note in the inset of figure 5, that both $H^*(T)$ and $H_{C2}(T)$ lines are well apart, so the change in VL mobility occurs far from the superconducting transition of the patterned film. The thickness of the corrugated Nb layer deposited on the V pillar array is probably not uniform, and this may also influence the VL pinning. Corrugation and thickness modulation may modify the pinning strength without modifying the matching conditions and, moreover, should not show any abrupt change with magnetic field.

The upper critical field $H_{C2}(T)$ of the sample (inset of figure 5 in blue circles) shows ΔT_c oscillations related to Little and Parks phenomena [19] at high temperature and the nonlinear temperature dependence indicates that near T_{C0} the superconducting coherence length is larger than the superconducting strips between V pillars [4].

Below $H^*(T)$ ($T^*(H)$), V pillars are superconducting. Pillars as antipinning centers in superconducting films have

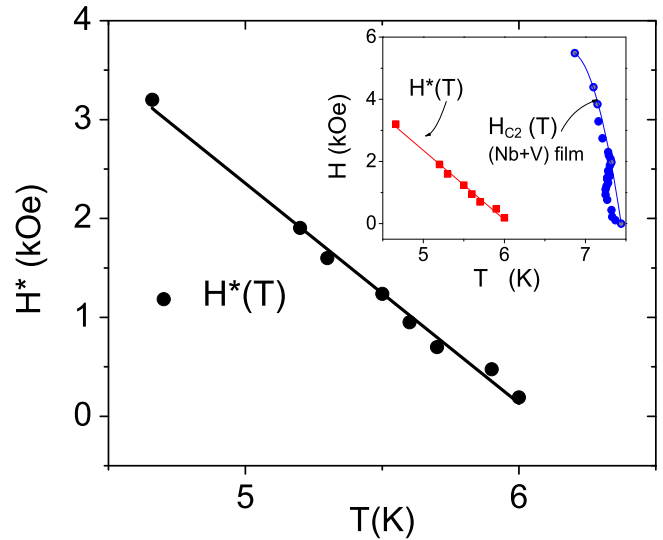


Figure 5. H^* versus T (black full circles; the line is a guide to the eye). The inset shows $H^*(T)$ and the sample $H_{C2}(T)$ in red full squares and blue full circles, respectively.

been studied [5] and have been shown to present matching effects [17]. Using the nonlinear Ginzburg–Landau theory, vortex configurations in a superconducting film with a square array of pillars in the presence of a uniform applied magnetic field was studied [5]. According to the radius, inter-pillar distance and thicknesses of pillars, different vortex structures were shown to be stabilized [5]. For a square array, vortices can be caged in interstitial positions, vortex chain structures may be formed as well as clusters of vortex molecules at the interstitial sites, depending on the applied magnetic field.

We were able to observe matching effects in antipinning landscapes, as mentioned above, for example at H_1 for $T = 4.7$ K, and at H_2 for $T = 3.9$ K (see figure 3), indicating that the VL is probably ordered and commensurate occupying interstitial positions, and as the number of vortices increases with applied field, the VL becomes more mobile. Additionally we conclude that for the particular geometry of our samples, antipinning seems more effective than pinning.

4. Conclusions

We examined, in ac susceptibility experiments, the vortex dynamics in Nb films containing a dense triangular array of submicrometric V pillars. We find matching effects for the first and second matching fields consistent with calculated matching fields for the triangular array of V pillars with a lattice parameter of 100 nm and an angular dependence indicating that the applied field normal component is relevant for matching. But the main result is the observation of an abrupt change in vortex mobility for a temperature dependent applied field, $H^*(T)$, that we find is consistent with the $H(T)$ superconducting to normal boundary field of V pillars. We present a scenario where below this field, pillars are superconducting and must therefore repel vortices, and interestingly, the VL responds with lower mobility than

above $H^*(T)$. Moreover, we observe matching at the first matching field at a low temperature where superconducting V pillars act as repulsive centers. Above $H^*(T)$, the V pillars become normal conventional pinning centers. Film corrugation may also contribute to pin the VL, but further work should be done to discriminate its contribution. In consequence, these samples are excellent candidates to disclose vortex dynamics as superconducting antipinning pillars turn into normal pinning centers. In this scenario, pinning by depression of the superconducting parameter, induced by proximity effects of normal V pillars and/or corrugation, is less effective than pinning by vortex repulsion by superconducting pillars for the particular geometry of our samples. A detailed comparison of the energies involved in each type of mechanism, the condensation energy due to the proximity of the normal pillars or the energy to create long or short vortices (vortex repulsion from pillars) and examination of samples with different geometries, will shed further light on the understanding of antipinning and pinning mechanisms.

Acknowledgments

We thank Juan Pereiro, Ilya Valmianski and Samuel A Hevia for their work in the porous alumina masks. We also thank Gabriela Pasquini, Carlos Acha and Julio Guimpel for helpful discussions and careful reading of the manuscript. This work was supported by PICT 2008 ANPCyT no. 0753 and UBA-CyT no. 661 and the US AFOSR grant no. FA9550-12-1-0381

References

- [1] Harada K, Kamimura O, Kasai H, Matsuda T, Tonomura A and Moshchalkov V V 1996 *Science* **274** 1167–70
- Moshchalkov V V, Baert M, Metlushko V V, Rosseel E, Van Bael M J, Temst K, Jonckheere R and Bruynseraede Y 1996 *Phys. Rev. B* **54** 7385
- Metlushko V *et al* 1999 *Phys. Rev. B* **60** 12585(R)
- Berdiyrov G R, Milošević V M and Peeters F M 2006 *Phys. Rev. Lett.* **96** 207001
- Berdiyrov G R, Milošević V M and Peeters F M 2006 *Phys. Rev. B* **74** 174512
- Welp U, Xiao Z L, Jiang J S, Vlasko-Vlasov V K, Bader S D, Crabtree G W, Liang J, Chik H and Xu J M 2002 *Phys. Rev. B* **66** 212507
- Patel U, Xiao Z L, Hua J, Xu T, Rosenmann D, Novosad V, Pearson J, Welp U, Kwok W K and Crabtree G W 2007 *Phys. Rev. B* **76** 020508(R)
- [2] Raedts S, Silhanek A V, Van Bael M J and Moshchalkov V V 2004 *Phys. Rev. B* **70** 024509
- [3] Lange M, Van Bael M J, Bruynseraede Y and Moshchalkov V V 2003 *Phys. Rev. Lett.* **90** 197006
- Milošević V M and Peeters F M 2005 *Europhys. Lett.* **70** 670
- Milošević V M, Yampolskii S V and Peeters F M 2002 *Phys. Rev. B* **66** 174519
- Milošević V M and Peeters F M 2003 *Phys. Rev. B* **68** 094510
- Jaccard Y, Martín J I, Cyrille M-C, Vélez M, Vicent J L and Schuller Ivan K 1998 *Phys. Rev. B* **58** 8232
- [4] Hoffmann A, Prieto P and Schuller Ivan K 2000 *Phys. Rev. B* **61** 6958
- [5] Berdiyrov G R, Misko V R, Milošević V M, Escoffier W, Grigorieva I V and Peeters F M 2008 *Phys. Rev. B* **77** 024526
- [6] Facio J I, Abate A, Guimpel J and Cornaglia P S 2013 *J. Phys.: Condens. Matter* **25** 245701
- [7] Bezryadin A, Ovchinnikov Y N and Pannetier B 1996 *Phys. Rev. B* **53** 8553
- [8] Li C-P, Roshchin I V, Battle X, Viret M, Ott F and Schuller Ivan K 2006 *J. Appl. Phys.* **100** 074318
- [9] Sekula S T and Kernohan R H 1972 *Phys. Rev. B* **5** 904
- [10] De Blois R W and De Sorbo W 1964 *Phys. Rev. Lett.* **12** 499
- [11] Poole C P, Farach H and Creswick R J 1995 *Superconductivity* (San Diego: Academic) p 65
- Koren G and Millo O 2009 *Phys. Rev. B* **80** 054507
- Koperdraad R T W and Lodder A 1995 *Phys. Rev. B* **51** 9026
- [12] Reichhardt C, Olson C J and Franco N 1998 *Phys. Rev. B* **57** 7937
- [13] Chliotte C, Pasquini G, Bekeris V, Li C P, Villegas J E and Schuller Ivan K 2011 *Supercond. Sci. Technol.* **24** 065008
- [14] Rosen Y J, Sharoni A and Schuller Ivan K 2010 *Phys. Rev. B* **82** 014509
- [15] Eisenmenger J, Oettinger M, Pfahler C, Plettl A, Walther P and Ziemann P 2007 *Phys. Rev. B* **75** 144514
- [16] Saint-James D 1965 *Phys. Lett.* **15** 13–15
- Moshchalkov V V, Qiu X G and Bruynseraede Y 1997 *Phys. Rev. B* **55** 11793
- Singha Deo P, Schweigert V A, Peeters F M and Geim A K 1997 *Phys. Rev. Lett.* **79** 4653
- Schweigert V A and Peeters F M 1998 *Phys. Rev. B* **57** 13817
- [17] Stoll O M, Montero M I, Guimpel J, Åkerman J J and Schuller Ivan K 2002 *Phys. Rev. B* **65** 104518
- [18] Morelle M, Golubović D S and Moshchalkov V V 2004 *Phys. Rev. B* **70** 144528
- [19] Little A W and Parks R D 1962 *Phys. Rev. Lett.* **9** 9